

# HiSST: 4th International Conference on High-Speed Vehicle Science Technology 22 -26 September 2025, Tours, France



# INVESTIGATING THE EFFECTS OF POROSITY ON THE DIELECTRIC AND MECHANICAL PROPERTIES OF ADDITIVELY MANUFACTURED CERAMICS

Louise SEVIN<sup>1</sup>, Waël IDRISSI<sup>2</sup>, Céline LE SINQ<sup>3</sup>, Johan PETIT<sup>4</sup>

#### **Abstract**

This study focuses on the electromagnetic properties of ceramics for ultra-high temperature radiofrequency (RF) windows. Although silica shows promising transparency properties due to its low dielectric constant ( $\epsilon$ ), its temperature limit (below 1373K) restricts its application. To overcome this limitation, we aim at reducing the dielectric constant of alternative ceramics while maintaining sufficient thermomechanical resistance. We investigated samples with various porosity levels (5-40%) and designs (gyroids, honeycombs, triangles, stars, and random porous structures) using Fused Deposition Modelling and conventional methods. Notably, our results align with established analytical models, yielding dielectric constants below 5 for porosities above 35%. Interestingly, the size of the interstices and walls (1500-5000  $\mu$ m) did not significantly affect the dielectric constant. Moreover, our findings highlight the importance of optimizing structured porosity to balance high flexural strength with reduced dielectric constant.

**Keywords**: Al<sub>2</sub>O<sub>3</sub>, Fused Deposition Modeling, electromagnetics properties, RF transparency

#### INTRODUCTION

Radomes protect antennas from increasingly aggressive environments while transmitting electromagnetic waves. It is imperative for hypersonic aircraft to have purposefully designed radomes, manufactured to withstand extreme conditions. Current commercially available materials for low-loss radiofrequency (RF) transmission offer limited performances when operating in the conditions associated with hypersonic flight. Silica and other silicate ceramics or glass ceramics exhibit very low dielectric constants ( $\epsilon$ ), facilitating good transparency properties; however, their use is restricted to temperatures below 1200°C due to thermal stability concerns. As alternatives to silica, researchers have investigated more refractory ceramic phases (as illustrated in Fig 1), which will be crucial for high-temperature applications. Some studies focus on developing lower dielectric constant phases or increasing porosity content to enhance electromagnetic properties.

Indeed, various materials, including  $Si_3N_4$  [1],  $Si_2N_2O$  [2], Y-SiAlON [3], mullite (3Al<sub>2</sub>O<sub>3</sub>-2SiO<sub>2</sub>) [4], multiphase material like BN-SiO<sub>2</sub> [5],  $Si_3N_4$ -BN-MAS [6] and aluminium phosphate-mullite [7] as composite material [8], [9] have been investigated for their composition's influence on dielectric properties.

<sup>&</sup>lt;sup>1</sup> ONERA/DMAS, Université Paris-Saclay, 29, avenue de la Division Leclerc - BP 72 - 92322 CHATILLON CEDEX, louise.sevin@onera.fr

<sup>&</sup>lt;sup>2</sup> ONERA/DMAS, Université Paris-Saclay, 29, avenue de la Division Leclerc - BP 72 - 92322 CHATILLON CEDEX, wael.idrissi@onera.fr

<sup>&</sup>lt;sup>3</sup> ONERA/DMAS, Université Paris-Saclay, 29, avenue de la Division Leclerc - BP 72 - 92322 CHATILLON CEDEX, celine.lesing@onera.fr

<sup>&</sup>lt;sup>4</sup> ONERA/DMAS, Université Paris-Saclay, 29, avenue de la Division Leclerc - BP 72 - 92322 CHATILLON CEDEX, johan.petit@onera.fr

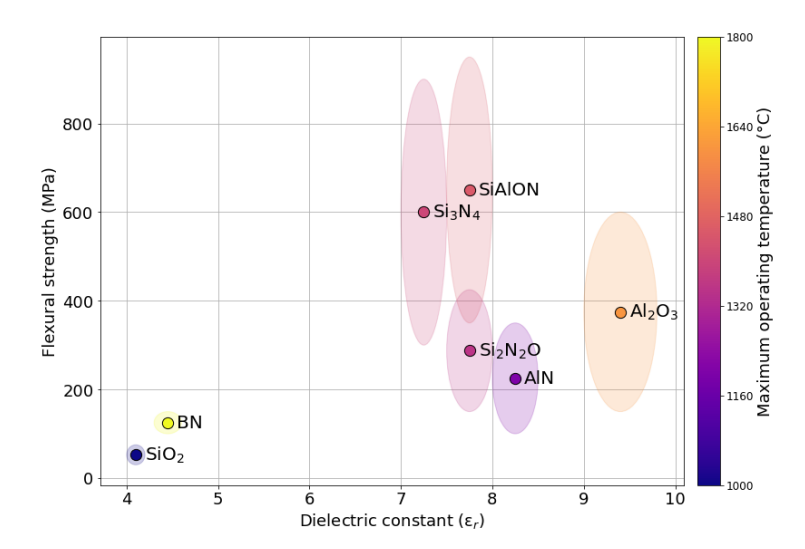


**Fig 1.** Flexural strength versus dielectric constant of ceramic materials with indication if service temperature, adapted from Zhou et al. [10]

Conversely, to lower the dielectric constant, authors have increased the porosity in both monolithic and composite materials. Penn et al. [11] demonstrated in the early 2000's the impact of the porosity, leading to a decrease in the dielectric constant of alumina from 10 down to 4.5 with 42% of porosity, whereas the tangent loss increased from  $3.10^{-5}$  to  $3.10^{-3}$  in the same time. In a Si<sub>3</sub>N<sub>4</sub>-SiO<sub>2</sub> multi-phase ceramic [12] with pore size ranging from 0.1 to 1  $\mu$ m, researchers observed a decrease in the dielectric constant from 3.8 (at 23% porosity) to 3.1 (at 42.5% porosity). This decrease is accompanied by an increase in loss tangent, which the authors attribute to the large surface area of the pores.

However, increasing porosity implies a decrease in mechanical resistance. The previous study showed that flexural strength lowers from 120 MPa (at 24% porosity) to 40 MPa (at 37% porosity), explained by the size and irregularity of the pores and sharp angles [12]. Yang et al. [13] demonstrated that, for 30% porosity, the flexural strength of silicon nitride is reduced by half compared to dense samples. Lastly, efforts to control porosity through freeze casting and gel casting of very porous Si<sub>3</sub>N<sub>4</sub> have yielded promising results: 100 MPa at 60% porosity and dielectric constant of 3.5 [14].

Thus, to conserve mechanical properties, while improving the dielectric properties, composite materials have been developed [10], [15], including  $Si_3N_4$  fibers with  $SiO_2$  matrix [16], which exhibited 160 MPa of flexural strength at room temperature (with 25% of open porosity). Additionally, 3D  $Si_3N_4$  fibers with BN- $Si_3N_4$  matrix [17] showed a flexural strength of 93 MPa at 8.5% open porosity and a dielectric constant of 5. A 2.5D SiNO fiber with BN matrix demonstrated an impressive flexural strength of 127 MPa at room temperature, with a dielectric constant of 3.4 [18].

These methods, however, have several disadvantages, notably the limited control over porosity, leading to non-uniform cellular structures that could affect material properties like flexural strength.

Today, Additive Manufacturing (AM) enables innovative solutions and breakthrough technologies for specific applications. However, for ceramics, this process is relatively new compared to its application in metals and polymers. Currently, high-quality ceramic parts are only achieved through multi-step additive manufacturing processes, which involve complex sequences of steps. In contrast, direct AM often results in parts with high crack density, attributed to the low toughness of ceramics under strong thermal gradients during the printing process. The production of the final part needs post-processing, typically involving in two to three steps, notably debinding (to remove binder materials) and sintering (to enhance densification and mechanical properties). The selection of the AM process depends on the size and resolution requirements of the part [19], [20], [21].

Given our research objective focuses on X-band electromagnetic and mechanical properties, the Fused Deposition Modeling (FDM) process' resolution (down to  $50~\mu m$ ) is deemed sufficient for our study. This process is versatile and can accommodate different ceramic compositions with very high loaded filaments [22]. Additionally, FDM allows for the design of open and closed porosity structures, as well

HiSST-2025-XXXX Page |

Copyright © 2025 by author(s)

as the processing of large-sized components [23], [24], offering advantages compared to stereolithography or Direct Light Processing (DLP) printing processes.

Therefore, our objective is to reduce the dielectric constant of porous ceramics while carefully maintaining sufficient thermomechanical resistance. To address this, samples with porosity ranging from 5 to 40% vol. were processed by two distinct processing methods: conventional methods involving a porogen agent and FDM 3D printing using an  $Al_2O_3$ -loaded filament.

#### **EXPERIMENTAL PROCEDURE**

# 1. Design of structures

First to structure the porosity, patterns were selected from the designs available in the slicer software used for 3D printing preparation. These structures include honeycombs, gyroids, stars, and triangles, as illustrated in Fig 2, with a base infill rate of 50% by volume. To achieve porosities ranging from approximately 40% to as low as 5% for the densest samples, the infill rate was varied between 20% and 100%. The achievable porosity range is influenced by the sample perimeter. Finally, the geometric dimensions of the pattern as the wall and gap widths are linked to the infill rate.

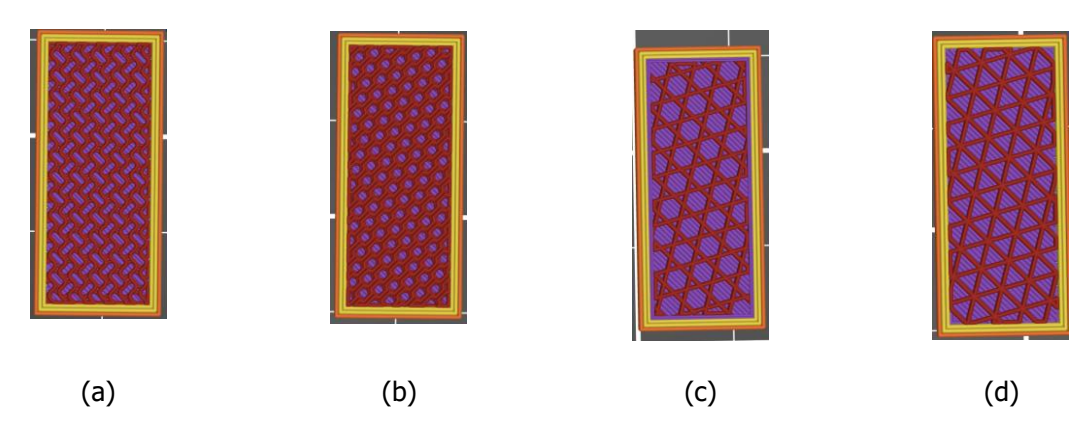


**Fig 2.** Representation of the patterns selected from the slicer at 50% infill rate: gyroids(a), honeycombs(b), stars(c) and triangles(c)

Additionally, specific honeycomb designs were created using CAD software, with a constant porosity of approximately 40% maintained across all variants. The number of hexagonal cells was reduced, while both the wall width and hexagon size were increased—from 0.4 mm to 2.4 mm and from 0.9 mm to 5.6 mm, respectively (Fig 3). Wide perimeters of 0.5 mm were added, slightly decreasing the overall sample porosity.

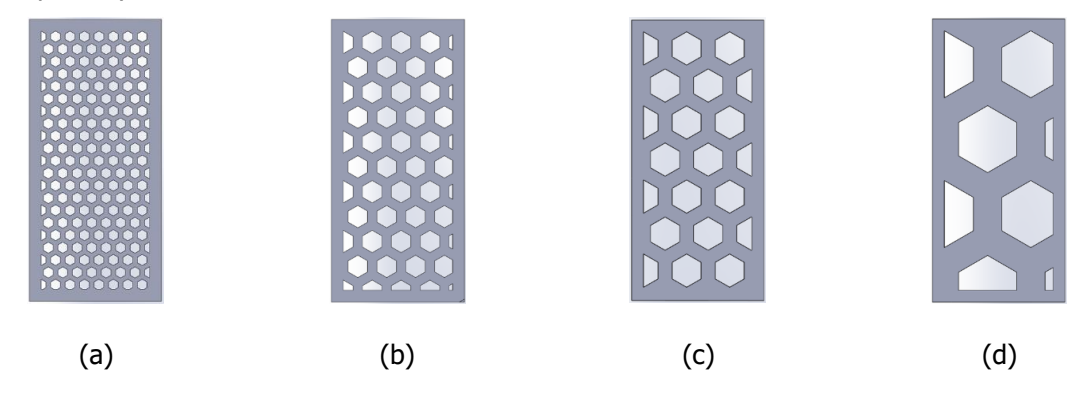


**Fig 3.** Representation of the different honeycombs with constant porosity of approximately 40 % and different hexagon & wall dimension: smaller size (a), medium low size (b), medium high size (c), higher size (d)

## 2. Processing

Structured porosity samples were printed using the Prusa Mk4S with Prusa Slicer (version 2.9.2) and a 0.4 mm diameter brass nozzle. The alumina-rich filament (D50 < 1  $\mu$ m) was supplied by Zetamix (Nanoe, France); the wire contains 83% alumina by weight. Printing and debinding parameters were set according to the supplier's recommendations, which included 4 h/mm in acetone bath set at 312 K, then heat treated at 773 K with a ramp of 8 K/h, and finally parts were sintered at 1873 K at 50 K/h under air.

For random porosity samples, commercially available ultrafine  $Al_2O_3$  powder (D50 < 0.2 µm, SM8 grade from Baikowski) was mixed with monodisperse PMMA pore formers (100 µm in diameter). The powder mixture was then poured into a square mold and uniaxially pressed at 80 MPa. The monodispersed PMMA was added in varying weight percentages: 0 wt.%, 15 wt.%, 30 wt.%, and 40 wt.% of the total mixture.

Both the 3D printed and uniaxially pressed green samples were sintered at a temperature of 1873K in an air atmosphere to achieve similar microstructural properties across both methods.

## 3. Characterization

## 3.1. Density

The density of the samples was determined by weighing the samples using a precision balance of  $10^{-4}$  g and measuring their dimensions to complete the density values. The procedure yields the geometrical density of the samples. The theoretical density of alumina is 3.99 g/cm<sup>3</sup> and was used as the reference value to calculate the relative density.

#### 3.2. Microstructural observations

To characterize the microstructural features of the samples (both FDM and randomly porous types), measurements were performed using an OLYMPUS GX71 optical microscope.

## 3.3. Dielectric constant

A vector network analyzer (ZNLE18, Rohde et Schwarz), coupled with a wave guide X11644A Hewlett Packard, was used to measure the transmission and reflection parameters ( $S_{11}$  et  $S_{21}$ ) in the frequency range (8-12 GHz). The real ( $\epsilon$ ') and imaginary ( $\epsilon$ ") parts of the permittivity were calculated using the Nicolson-Ross-Weir method [25]. The sample dimensions were 23 x 11 x 3 mm<sup>3</sup>.

## 3.4. Flexural strength

Four-point bending tests were conducted at ambient temperature to determine the flexural strength. Rectangular bars with dimensions of  $3 \times 4 \times 45$  mm<sup>3</sup> were machined for testing. The loading rate was set to 0.5 mm·min<sup>-1</sup>, with a span length of 20 mm. At least three specimens were tested, and the average values were reported in MPa are calculated from (1, where F is the fracture force in Newtons, L the outer span (mm), I the inner span (mm), b the test piece width (mm) and h the test piece height (mm).

$$\sigma_f = \frac{3F(L-l)}{2bh^2} \tag{1}$$

## **RESULTS**

## 4. Microstructure of resulting patterns

## 4.1. Random porosity samples

As shown in Fig 4, increasing the amount of PMMA spheres results in higher porosity and promotes the formation of agglomerates, leading to large void regions and walls with wide variation in thickness.

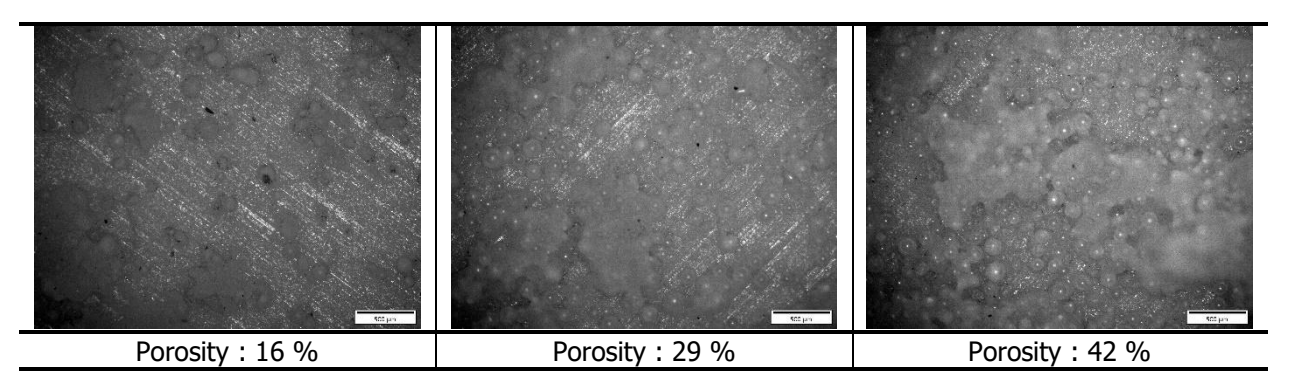


Fig 4. Observations of the microstructure of random porous samples function of the porosity

# 4.2. Structures shaped with slicer

The Table 1 shows the microstructural observations of the structured design with the slicer software for the gyroids, honeycombs, stars, and triangles. The infill rate from 85% to 40% lead to samples with 13 to 39.2%.

**Table 1** Observations and effective porosity (considering perimeters and intercordon porosity) function of the infill rate of structured samples with gyroids, honeycombs, stars and triangles

Infill rate	Gyroids	Honeycombs	Stars	Triangles
85%	15%		14.4%	13.4%
70%	23.6%	19.2%	19.1%	20.6%
55%	31.2%	26.8%	26.2%	24.5%
40%	39.2%	35.0%	35.2%	34.2%

To complement the initial observations, the sizes of the gaps and walls in each sample were measured and analyzed in relation to porosity (Fig 5). Of the different patterns, the gyroid structure exhibits the smallest feature sizes. As porosity increases, the interstice size increases, while the wall width tends to decrease. In the case of honeycombs, the hexagonal shape is not clearly defined; the structure appears to adopt a diamond-like geometry along the z-axis. For these samples, both the interstice size and the wall thickness increase with porosity. In the triangular pattern, the interstice size increases with Page |

porosity, while the wall width remains constant. For the star-shaped structures, the interstice size increases, while the wall thickness decreases. This pattern results in the largest structure size. Overall, the interstice sizes across all structures range from 100 to 1500  $\mu$ m, and the wall widths range from 125 to 400  $\mu$ m.

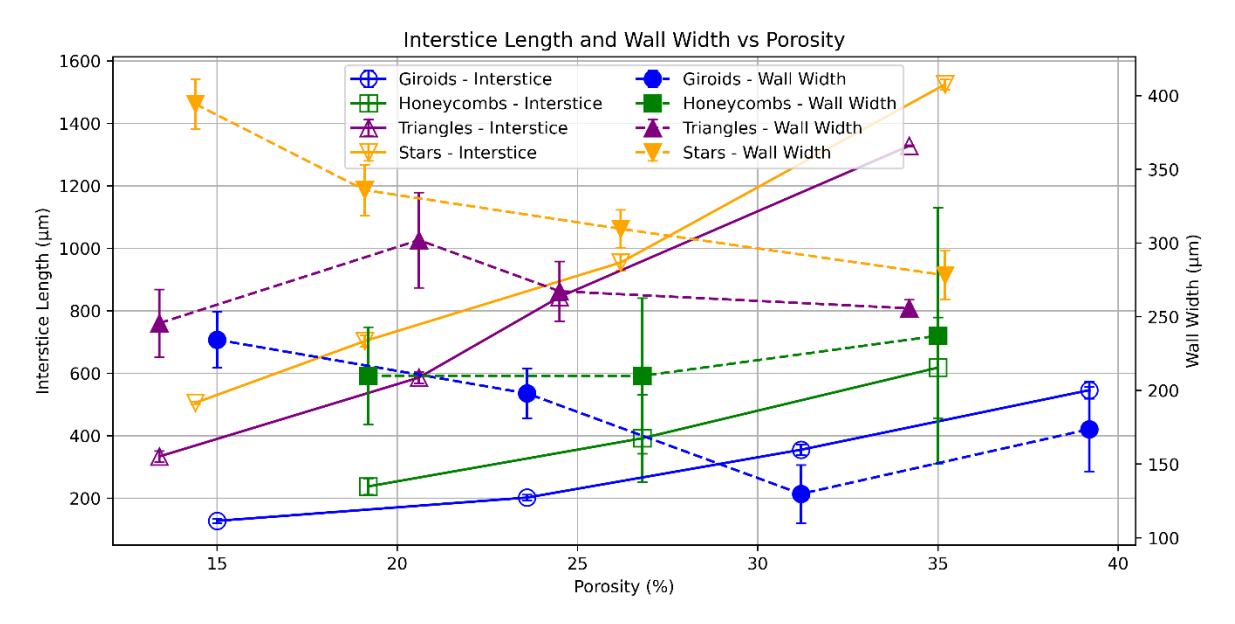


**Fig 5.** Comparison of structured size function of porosity for structured generated by the slicer: gyroids, honeycombs, stars, triangles

# 4.3. Structures shaped with CAD software

As described in Section 2.1, honeycombs structures were precisely designed using CAD software to investigate the effect of their size on dielectric properties at a constant porosity. The microstructure of the samples is shown in Fig 6. The sample with the finest honeycomb structure revealed limitations of the printing process, as the printer was unable to accurately reproduce the fine hexagonal geometry, resulting in partial infill along the printer's return path. This leads to a lower porosity of 29.6% compare to the other samples which reach a porosity range from 37.5 to 41.5%. The interstice lengths range from 1800 to 5000 µm, while the wall widths vary between 750 and 2250 µm.

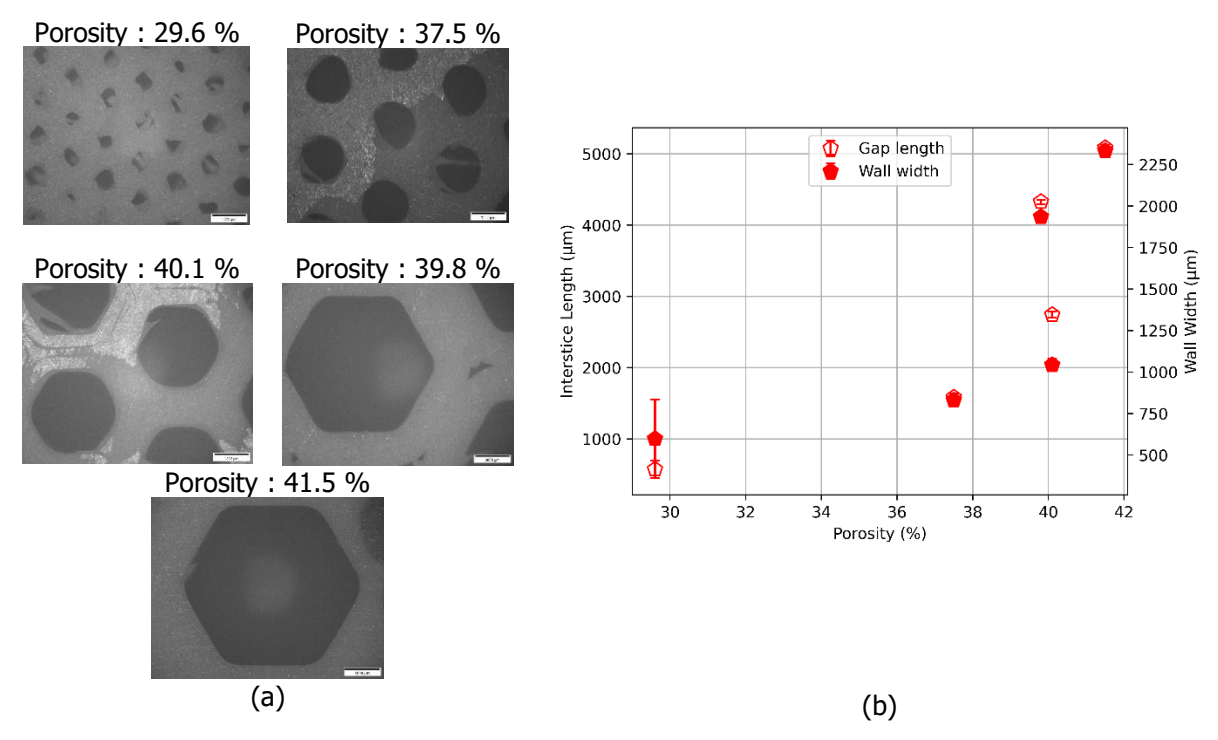


**Fig 6.** Structures micrographics of CAD designed honeycombs with constant resulting porosity, around 40% (a) and their relative geometric dimensions (b)

# 5. Dielectric properties

The figure below plots (Fig 7) the measured dielectric constant is plotted as a function of porosity for different structured porosities, gyroids, honeycombs, triangles, and stars, processed using the slicer, as well as for randomly porous samples produced using a conventional method. These results are compared with literature data from Penn et al. [11]. All the datasets, except those from the randomly porous samples, can be reasonably fitted with a linear approximation, with correlation coefficients greater than 0.9. Additionally, the Heidinger approximation [26] is overlaid on the figure and shows good agreement with the data, regardless of the type of porous structure used.

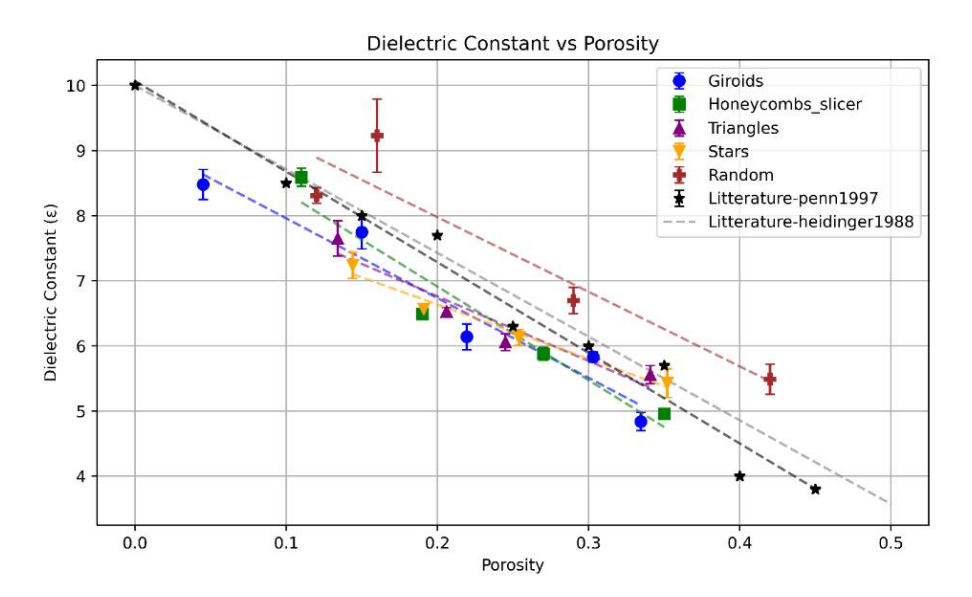


**Fig 7.** Dielectric constant as a function of porosity for various structured porous materials, including gyroids, honeycombs, triangles, and stars fabricated via slicer-based 3D printing, and randomly porous samples produced by conventional methods.

Next, we compared the dielectric constants of CAD-designed honeycombs with those of honeycombs generated by a slicer (Fig 8 (a)). Both sets show excellent agreement with the literature data. The 42% porosity sample exhibits a dielectric constant of 5.2 which is slightly higher than that of the other samples around 40% of porosity. To better observe the evolution of the dielectric constant as a function of structural size while maintaining constant porosity, the 30% porosity sample was excluded. The figure below (Fig 8(b)) shows the dielectric constant plotted against interstice length and wall width for CAD-designed honeycomb samples with porosities ranging from 38% to 42%. Its structure size features the largest interstice length and wall width (Fig 8 (b)), measuring approximately 5000  $\mu$ m and 2300  $\mu$ m, respectively. These dimensions are close to the wavelength of the measured electromagnetic waves, which may explain this atypical behaviour, a phenomenon that has rarely been studied.

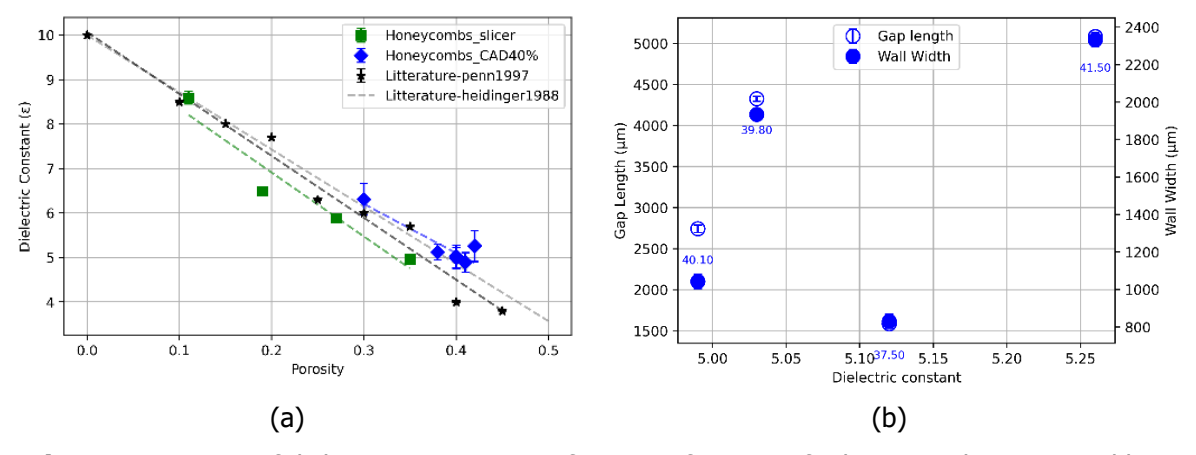


**Fig 8.** Comparison of dielectric constant as a function of porosity for honeycombs generated by slicer software and gyroids designed with CAD software (a), Comparison of dielectric constant function of gap length and wall width of CAD honeycombs (b)

## 6. Mechanical properties

As predicted by Kwan et al. [27], randomly porous samples exhibit decreased flexural strength as porosity increases. At 33% of porosity, the flexural strength is 20 MPa (see Fig 9) which is far too low for the intended application. The next stage of the study will involve printing a structured pattern with a relatively high flexural strength, which will then be compared with this set of data.

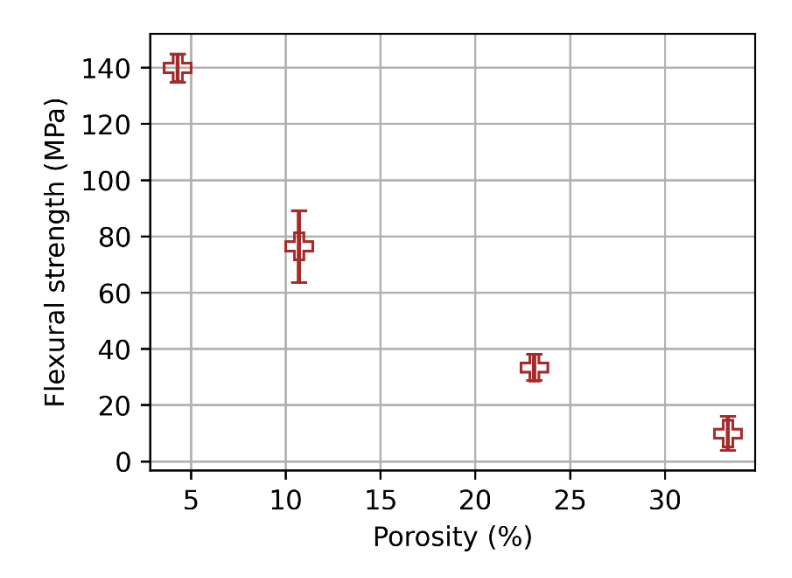


Fig 9. Mechanical properties of random porous samples function of porosity (4 to 33%)

#### **CONCLUSIONS AND PERSPECTIVES**

This study demonstrates the possibility of designing patterns in the dielectric properties of alumina-based materials. Various structured porosities, including gyroids, honeycombs, stars and triangles, were successfully fabricated using slicer- and CAD-based approaches, which enable precise control over porosity and feature size. The dielectric constant was shown to decrease with increasing porosity, which is consistent with existing literature and can be well described by established models, such as the Heidinger approximation. Notably, CAD-designed gyroids with larger interstice lengths and wall widths exhibited a slightly higher dielectric constant, likely due to interactions with electromagnetic wavelengths. This highlights the importance of structural scale in relation to the measurement frequency.

Mechanical testing confirmed that the flexural strength of randomly porous samples decreased significantly with increasing porosity, emphasising the trade-off between lightweight design and mechanical performance. The ability to tailor pore size and geometry at a given porosity offers a promising approach to optimising material properties for applications requiring specific dielectric or mechanical characteristics.

Future work should explore the interplay between structural dimensions and wave-material interactions in greater detail, as well as investigating the scalability and reproducibility of these architectures for application.

## **REFERENCES**

- [1] J. Walton, « Reaction Sintered Silicon-Nitride for High-Temperature Radome Applications », *Am. Ceram. Soc. Bull.*, vol. 53, n° 3, p. 255-258, 1974.
- [2] J. Barta, M. Manela, et R. Fischer, « Si3N4 and Si2N2O for high performance radomes », *Materials Science and Engineering*, vol. 71, p. 265-272, mai 1985, doi: 10.1016/0025-5416(85)90236-8.
- [3] R. Yang *et al.*, « High wave transmittance and low thermal conductivity Y-a-SiAlON porous ceramics for high-temperature radome applications », *Journal of Advanced Ceramics*, vol. 12, n° 6, p. 1273-1287, juin 2023, doi: 10.26599/JAC.2023.9220756.

- [4] N. Ecebaş, G. M. Dursun, A. H. Yeşilova, et C. Duran, « Gel casting of mullite for radome applications », *International Journal of Applied Ceramic Technology*, vol. 17, nº 1, p. 264-273, 2020, doi: 10.1111/jjac.13269.
- [5] Q. Li *et al.*, « Effect of the BN content on the thermal shock resistance and properties of BN/SiO 2 composites fabricated from mechanically alloyed SiBON powders », *RSC Advances*, vol. 7, n° 77, p. 48994-49003, 2017, doi: 10.1039/C7RA09905C.
- [6] W. Zou *et al.*, « Effect of boron nitride content on mechanical、dielectric and thermal shock resistance properties of Si3N4-BN-MAS composites », *Ceramics International*, vol. 50, nº 17, Part A, p. 29866-29876, sept. 2024, doi: 10.1016/j.ceramint.2024.05.282.
- [7] Y. Wang et J. Liu, « Aluminum Phosphate–Mullite Composites for High-Temperature Radome Applications », *International Journal of Applied Ceramic Technology*, vol. 6, nº 2, p. 190-194, 2009, doi: 10.1111/j.1744-7402.2008.02324.x.
- [8] R. Cass, G. Eadon, et P. Wentzel, « Processing and Properties of Fiber Reinforced Barium Aluminosilicate Composites for High Temperature Radomes », in *Mechanical Properties and Processing of Ceramic Binary, Ternary, and Composite Systems: Ceramic Engineering and Science Proceedings, Volume 29, Issue 2*, John Wiley & Sons, Ltd, 2008, p. 179-187. doi: 10.1002/9780470456361.ch17.
- [9] Y.-G. Jiang, C.-R. Zhang, F. Cao, S.-Q. Wang, H.-F. Hu, et G.-J. Qi, « Fabrication of High Performance 2.5D SiO2f/Si3N4-BN Composites for High-temperature Application », *Advanced Engineering Materials*, vol. 9, n° 1-2, p. 114-116, 2007, doi: 10.1002/adem.200600108.
- [10] J. Zhou *et al.*, « Development of high-temperature wave-transparent nitride-based CFCMCs for aircraft radomes », *Composites Part A: Applied Science and Manufacturing*, vol. 167, p. 107444, avr. 2023, doi: 10.1016/j.compositesa.2023.107444.
- [11] S. J. Penn *et al.*, « Effect of Porosity and Grain Size on the Microwave Dielectric Properties of Sintered Alumina », *Journal of the American Ceramic Society*, vol. 80, nº 7, p. 1885-1888, 1997, doi: 10.1111/j.1151-2916.1997.tb03066.x.
- [12] X. Li, X. Yin, L. Zhang, L. Cheng, et Y. Qi, « Mechanical and dielectric properties of porous Si3N4–SiO2 composite ceramics », *Materials Science and Engineering: A*, vol. 500, n° 1, p. 63-69, janv. 2009, doi: 10.1016/j.msea.2008.09.066.
- [13] J.-F. Yang, T. Ohji, S. Kanzaki, A. Díaz, et S. Hampshire, « Microstructure and Mechanical Properties of Silicon Nitride Ceramics with Controlled Porosity », *Journal of the American Ceramic Society*, vol. 85, n° 6, p. 1512-1516, 2002, doi: 10.1111/j.1151-2916.2002.tb00305.x.
- [14] H. Zhang *et al.*, « A comparative study on dielectric and mechanical properties of porous β-Si3N4 ceramics by controlling porosity and microstructure », *Journal of the European Ceramic Society*, vol. 42, n° 3, p. 905-912, mars 2022, doi: 10.1016/j.jeurceramsoc.2021.11.004.
- [15] Y. Wang, Z. Peng, R. Tian, G. Luo, W. Fan, et J. Zhang, « Microwave-transparent refractory materials for high-temperature metallurgical applications », *Journal of Alloys and Compounds*, vol. 1033, p. 181063, juin 2025, doi: 10.1016/j.jallcom.2025.181063.
- [16] X. Yang, B. Li, D. Li, C. Shao, et C. Zhang, « High-temperature properties and interface evolution of silicon nitride fiber reinforced silica matrix wave-transparent composite materials », *Journal of the European Ceramic Society*, vol. 39,  $n^{\circ}$  2, p. 240-248, févr. 2019, doi: 10.1016/j.jeurceramsoc.2018.09.007.
- [17] J. Zhou *et al.*, « Effects of heat treatment on mechanical and dielectric properties of 3D Si3N4f/BN/Si3N4 composites by CVI », *Journal of the European Ceramic Society*, vol. 40, n° 15, p. 5305-5315, déc. 2020, doi: 10.1016/j.jeurceramsoc.2020.06.018.
- [18] C. Zou, C. Zhang, B. Li, S. Wang, Z. Xie, et Y. Song, « Fabrication and properties of borazine derived boron nitride matrix wave-transparent composites reinforced by 2.5 dimensional fabric of Si–N–O fibers », *Materials Science and Engineering: A*, vol. 620, p. 420-427, janv. 2015, doi: 10.1016/j.msea.2014.10.046.

- [19] J. Binner *et al.*, « Selection, processing, properties and applications of ultra-high temperature ceramic matrix composites, UHTCMCs a review », *International Materials Reviews*, vol. 65, n° 7, p. 389-444, oct. 2020, doi: 10.1080/09506608.2019.1652006.
- [20] T. G. Aguirre, C. L. Cramer, et D. J. Mitchell, « Review of additive manufacturing and densification techniques for the net- and near net-shaping of geometrically complex silicon nitride components », *Journal of the European Ceramic Society*, vol. 42, n° 3, p. 735-743, mars 2022, doi: 10.1016/j.jeurceramsoc.2021.11.001.
- [21] Y. Lakhdar, C. Tuck, J. Binner, A. Terry, et R. Goodridge, « Additive manufacturing of advanced ceramic materials », *Progress in Materials Science*, vol. 116, p. 100736, févr. 2021, doi: 10.1016/j.pmatsci.2020.100736.
- [22] « Additive manufacturing of silicon nitride ceramics: A review of advances and perspectives Dong 2022 International Journal of Applied Ceramic Technology Wiley Online Library ». Consulté le: 3 mars 2023. [En ligne]. Disponible sur: https://ceramics.onlinelibrary.wiley.com/doi/full/10.1111/ijac.14162
- [23] F. Clemens, F. Sarraf, A. Borzì, A. Neels, et A. Hadian, « Material extrusion additive manufacturing of advanced ceramics: Towards the production of large components », *Journal of the European Ceramic Society*, vol. 43, n° 7, p. 2752-2760, juill. 2023, doi: 10.1016/j.jeurceramsoc.2022.10.019.
- [24] S. Iyer *et al.*, « Microstructural Characterization and Mechanical Properties of Si3N4 Formed by Fused Deposition of Ceramics », *International Journal of Applied Ceramic Technology*, vol. 5, n° 2, p. 127-137, 2008, doi: 10.1111/j.1744-7402.2008.02193.x.
- [25] E. J. Rothwell, J. L. Frasch, S. M. Ellison, P. Chahal, et R. O. Ouedraogo, « Analysis of the Nicolson-Ross-Weir method for characterizing the electromagnetic properties of engineered materials », *Progress In Electromagnetics Research*, vol. 157, p. 31-47, 2016.
- [26] R. HEIDINGER, « Ceramic materials for microwave windows », *International Journal of Electronics*, vol. 64, n° 1, p. 37-48, janv. 1988, doi: 10.1080/00207218808962783.
- [27] Y. B. P. Kwan, D. J. Stephenson, et J. R. Alcock, « The porosity dependence of flexural modulus and strength for capsule-free hot isostatically pressed porous alumina », *Journal of Materials Science*, vol. 35, n° 5, p. 1205-1211, mars 2000, doi: 10.1023/A:1004792605528.